AAS-05-4185

AUGMENTATIONS TO THE POLYHEDRAL GRAVITY MODEL TO FACILITATE SMALL BODY NAVIGATION

L. Alberto Cangahuala

Jet Propulsion Laboratory
California Institute of Technology
Pasadena, California

AAS-05-4185

AUGMENTATIONS TO THE POLYHEDRAL GRAVITY MODEL TO FACILITATE SMALL BODY NAVIGATION

L. Alberto Cangahuala♦

Abstract - One of the challenges in modeling low-altitude mission scenarios at small bodies is the need to minimize the computation time penalty for more detailed shape models, especially when the scale of the detail is on the order of the spacecraft trajectory. This paper describes variants of the polyhedral model and their relative performance. Variations include (a) using approximations to the more computationally intensive terms in the acceleration and partial calculations, (b) using approximations for sums of terms that are disproportionately detailed, and (c) simply using a simpler reference polyhedron. Accuracy and speed performance assessments are made for these variations for three cases: (a) an aggressive mapping orbit, (b) low altitude hovering, and (c) disturbances of regolith material at the surface of an asteroid. Analogous results are also shown for spherical harmonics and a three-axis ellipsoid.

The results show that the benefits to using Taylor series approximations and carrying the history of calculations from a previous call to a nearby point can range from 30 to 60 percent for each augmentation. The accuracy penalty for these augmentations is smaller than the uncertainties in the gravity field itself, so they warrant being included in gravity model software sets.

INTRODUCTION

Future small body mission designs require close-proximity trajectory analyses of the spacecraft and particles lifted from the surface due to intentional and unintentional spacecraft activity. Accurate gravity modeling in particular drives the overall modeling accuracy of these close orbits, landings and ascents. This dependency can be somewhat mitigated through the introduction of closed-loop flight path control, but there are science scenarios involving (a) passive science pods on the surface, or (b) low-velocity ejecta that continue to reinforce the need for such modeling.

For the above scenarios, low-altitude gravity modeling must also be supplemented by a realistic and (wherever possible) accurate surface reference. This combination is needed in order to compute accurate surface contact footprint and timing estimates, as well as disturbed particle distribution pattern estimates. Surface references usually come from scientists in the form of a

♦ Technical Group Supervisor, Jet Propulsion Laboratory / California Institute of Technology, 4800 Oak Grove Drive, Pasadena CA 91109-8099, E-mail:albe@jpl.nasa.gov

polyhedron shape model. By assuming that the body is homogeneous, one can use the shape model as the foundation for a gravity field as well.[1]

One of the challenges with using a polyhedral gravity field is to minimize the computation time penalty for more detailed shape models, especially when the scale of the detail is on the order of the spacecraft dimensions. A second challenge is to preserve the surface relief modeling around potential landing areas to facilitate compiling more detailed landing or contact statistics. This paper describes variations of the polyhedral model and their relative performance attributes.

The variations considered here are approximations to the more computationally intensive terms or disproportionately detailed terms in the acceleration and partial calculations. Representative versions of the model variations are defined, and their use in precision numerical integrations is described. Representative cases include (a) a spacecraft (or a binary companion in a low orbit about an asteroid, (b) a spacecraft hovering at a low altitude over the surface of a small body, and (c) the redistribution of dust particles of varying sizes across the surface in response to a spacecraft making contact with the surface. The trajectories are modeled using scripts that supplement the core capabilities of JPL's MONTE program. MONTE is an accurate and general-purpose trajectory program that can model many relevant force perturbations found in the solar system to high levels of precision.

The key objective of this work is to describe polyhedral gravity framework that has the flexibility to be used on a variety of small body targets without much retooling, and that the computational efficiency enables mission designers and navigation analysts to focus on other, less standardized models which may affect the spacecraft (comet outgassing) or near-surface particle (ejecta distribution, static charges) trajectories.

In the following section three scenarios at small bodies are described. The gravity modeling section covers the baseline polyhedral model, along with the proposed variations. This is followed by the test descriptions and setup, and finally, the results.

SMALL BODY SCENARIOS

The objective of scenario selection is to find a small set of cases that (a) is relevant to small body mission science objectives, (b) spans a variety of relative speeds, orbit energies, and surface coverage, and (c) can be applied not only to the investigating spacecraft, but also to particles of different sizes that one might encounter upon arrival.

Mapping Orbits

One scenario that is part of missions to all but the tiniest of small body objects is an orbital mapping phase. These phases are usually planned to last from 2 weeks to 2 months in duration. Mapping orbit selection itself a tradeoff between the operational simplicity and robustness of a larger orbit versus the improved coverage rate and feature resolution available with a smaller orbit. The key considerations that result in upper and lower limits to orbit size (Ref. 2) include

[1] Casotto and Musotto give an excellent overview and characterization of gravity models as applied to small bodies in (Ref. 1).

- The maneuver execution error floor,
- The Ratio of the magnitudes of gravitational acceleration to solar radiation acceleration,
- The small body rotation period and ellipticity, and
- Solar radiation versus oblateness perturbations.

In order to more easily depict some example orbit selections, the target asteroid semi-major axis is set to 1 AU, the spacecraft area to mass ratio is 40 kg/m^2, the asteroid density is 2.5 g/cm^3, and the spin axis direction to within a few degrees of the asteroid terminator plane (other spin directions are considered in the next section). Figure 1 shows the effects that define the upper and lower bounds for mapping orbit size for asteroids whose masses range from μ of 10^{-9} to 10^{-3} km^3/s^2 (with the Muses-C target Itokawa noted). As a reference, traces of 3 and 10 mean asteroid radii are included as a function of asteroid mass, as well as the NEAR 35km science orbit around Eros.

Figure 1. Mapping Orbit Size Constraints

One upper limit on orbit size, especially for smaller asteroids, is the ratio of gravitational acceleration over solar radiation acceleration. As this ratio drops, the time-averaged orbit plane becomes offset from the asteroid center, and it may not be possible to obtain complete radar coverage of the asteroid. Figure 1 shows the allowable orbit sizes for a ratio of 10:1. Another upper bound on orbit size for smaller targets is the ability of the propulsive system to properly place the spacecraft into the mapping orbit. The maneuver execution error floor should remain a small fraction (1-2%) of the orbital velocity in order to have a reasonable chance of safely entering and exiting those mapping orbits. Figure 1 also shows the allowable orbit sizes for mean orbit velocities of 5 and 10 cm/s.

The orbit size dynamical lower limit is due to the irregular shape of the asteroid. The oblateness has no direct secular effect on orbit size or eccentricity. The ellipticity, however, can lead to instabilities which act on the orbit eccentricity, placing the spacecraft on an escape or crash trajectory. To mitigate this possibility, spacecraft are placed in retrograde orbits, and near-synchronous orbits and orbits resonant with the asteroid's particular elliptical profile are avoided. The dashed traces in Figure 1 show the orbit sizes for a family of orbit periods. Since the majority of asteroid rotation periods are in the range of 5 to 10 hours, setting the lower orbit size limit so that the resulting orbit period is greater than 24 hrs will keep most mapping orbits out of phase with the asteroid shape perturbations. This results in orbit sizes on the order of 3-6 mean radii.

Another interesting property of this orbit size is that it can be representative of the orbit sizes of small binary objects also orbiting the primary body, which would be of interest to mission designers. While these objects do not naturally remain in such controlled orbits, they are subject to the same effects as artificial satellites (albeit with a higher solar ballistic coefficient), and particles whose orbit sizes significantly exceed these bounds will not last long as binary objects.

Hovering

Inertial hovering is an enabling strategy for observing small bodies, especially those with very small masses ($\mu < 10^{-8}$ km^3/s^2). Typical techniques considered to maintain the desired distance use imaging and ranging against the entire body, so the standoff distances are typically

several radii in size, distances greater than the mapping orbit sizes described in the previous section.

Body-fixed hovering is a strategy that can enhance the science return of surveys of candidate landing or sampling sites. With this approach one can remain at short distances from the area of interest for longer periods of time than are possible with multiple flybys. The navigation strategy in this case also relies on optical data and altimetry, but the images usually only cover a few percent of the total surface area at any time. The tradeoff here is between minimizing the distance to the area of interest, and minimizing the introduction of additional activity (slewing, hazard avoidance, thruster contamination of the surface) that might add significant risk or diminish science return. For scenario development a 24-hour hovering campaign is considered (long enough to allow the ground in the loop for one update to the observation profile), and a standoff distance of a quarter of the mean radius is used.

Sampling

There are many sampling mechanisms being considered for asteroid and comet sample return missions, including scoops, brushes, drills, and coring devices. Two attributes that most of them have in common are (a) either the sampling mechanism itself or its housing will inadvertently disturb particles near the actual sample, and (b) the velocities involved between the sampling device and the uncollected surface material will be sufficient to place some fraction of these particles into trajectories that traverse a significant fraction of the small body. These qualities can also be attributed to landing dynamics as well.

This study does not intend to cover the wide variety of possible low-velocity ejecta profiles. However, there is a need to assess the impact (literally) of inadvertently lifted particles on the spacecraft. Thus, a representative case needs to be defined to show the impact of different gravity models on the forecasted trajectories. For the sake of scenario development, a scoop-like sampling device disturbs a parcel of regolith. The uncollected particles move in nearly the same direction away from the spacecraft at a low angle of incidence to the local surface, at less than escape velocity.

GRAVITY MODELS

In this section we define the polyhedral gravitational potential, attraction, and gravity gradient, then describe the proposed augmentations.

Polyhedron Method

Using the notation in (Ref. 3) and Figure 2:

Figure 2. Polyhedron Triangular Face/Vertex Diagram (L), Face, Edge Normals (R)

$$U = \frac{1}{2} G\sigma \left[\sum_{e \in edges} r_e \bullet E_e \bullet r_e \cdot L_e - \sum_{f \in faces} r_f \bullet F_f \bullet r_f \cdot \omega_f \right] \tag{1}$$

$$\Delta U = -G\sigma\left[\sum_{e\in edges} E_e \bullet r_e \cdot L_e + \sum_{f\in faces} F_f \bullet r_f \cdot \omega_f\right] \tag{2}$$

$$\Delta\Delta U = G\sigma\left[\sum_{e\in edges} E_e \cdot L_e - \sum_{f\in faces} F_f \cdot \omega_f\right] \tag{3}$$

where for each edge,

$$L_e = \ln\frac{r_i + r_j + e_{ij}}{r_i + r_j - e_{ij}} \tag{4}$$

and ω_f is the solid angle for each face,

$$\omega_f = 2\tan^{-1}\left(\frac{r_i \bullet r_j \times r_k}{r_i r_j r_k + r_i\left(r_j \bullet r_k\right) + r_j\left(r_k \bullet r_i\right) + r_k\left(r_i \bullet r_j\right)}\right) \tag{5}$$

and E_e and F_f are dyads formed from the face and edge normals:

$$E_e\big|_{P_1,P_2} = \hat{n}_A\hat{n}_{12}^A + \hat{n}_B\hat{n}_{21}^B \qquad F_f = \hat{n}_f\hat{n}_f \tag{6, 7}$$

The Laplacian is also of special interest, as it can be used to determine whether the particle of interest is outside or inside the polyhedron:

$$\nabla^2 U = -G\sigma\sum_{f\in faces}\omega_f \tag{8}$$

Taylor Series Approximations

The original algorithm has been coded for many applications that appear in the literature[2]. Profiling these implementations using relevant test cases is the proper manner to identify improvements that can be made without sacrificing any performance at all. Assuming that has been done, one obvious step to consider is to minimize the computations that go into each of the terms of equations (1)-(3). In particular, computation of logarithms and arctangents take longer than the surrounding matrix and vector multiplications[3]. The function calls in equations (4) and (5) can be replaced by their one-term and two-term Taylor series approximations:

[2] Robert Werner, personal communication.

[3] Pohánka first focused on these terms in (Ref. 4) as a source of speed enhancement, but for a slightly different formulation of the polyhedral gravity field.

$$L_e \approx 2\frac{e_{ij}}{r_i + r_j} \qquad L_e \approx 2\left(\frac{e_{ij}}{r_i + r_j} + \frac{1}{3}\left(\frac{e_{ij}}{r_i + r_j}\right)^3\right) \tag{7a, b}$$

$$\omega_f \approx 2\left(\frac{n_{ijk}}{d_{ijk}}\right) \qquad \omega_f \approx 2\left(\frac{n_{ijk}}{d_{ijk}} - \frac{1}{3}\left(\frac{n_{ijk}}{d_{ijk}}\right)^3\right) \tag{8a, b}$$

$$n_{ijk} = r_i \bullet r_j \times r_k \qquad d_{ijk} = r_i r_j r_k + r_i\left(r_j \bullet r_k\right) + r_j\left(r_k \bullet r_i\right) + r_k\left(r_i \bullet r_j\right) \tag{9 a, b}$$

The resulting errors for one-term and two-term L_e and ω_f approximations are on the order of (e_{ij}/r_i+r_j) and (n_{ijk}/d_{ijk}) to the third and fifth powers, respectively. In the code, these approximations only take effect these ratios go below a certain value (0.1 in these tests).

Face/Edge Histories

The next level of computation consolidation is to consider approximations for groups of terms for the faces and edges that are far from the object. Another possibility, which would be beneficial to cases where the object motion is limited to a small fraction of the polygon, is to leverage off of the computations performed in the previous iteration. One can carry histories of (e_{ij}/r_i+r_j) for each edge, and the signed distance to each face, and update the L_e and ω_f computations only if the current values exceed a particular threshold.

Coarser Shape Representations

Another simplification is to use a coarser shape representation. The addition of the Taylor series approximations on a more coarse shape leads to larger errors in L_e (the edges grow while r_i, r_j remain the same), but smaller errors in ω_f (the solid angle described by r_i, r_j, and r_k, which remain constant, grows). For the mapping orbit cases, the L_e errors should dominate.

TESTS

This section describes the numerical experiments performed to evaluate the performance of the original polyhedral model as well as the variations for the selected small body scenarios.

Setup

While small body masses span several orders of magnitude, rather than repeat the evaluations over multiple bodies, a mass of $\mu = 3(10^{-8})$ km^3/s^2 was selected and placed in a NEO-like orbit. A smaller mass would obviate the need for a mapping orbit scenario. A larger mass would make it easier to see the effects of gravity mismodeling on the mapping orbit, but at this size, variations in the surface dust dynamics would be easier to evaluate. Since there have been fewer studies of dust dynamics in the literature, it was decided to focus on a body of this size.

As with the small body mass, there are many shape models available, both derived from direct and radar observations, as well as simulated. The shapes reflect different assumptions about (a) the amount and distribution of regolith material, (b) the amount and distribution of

volatile material near the surface, and (c) the impact history upon the body, and (d) the internal homogeneity of the body itself. For these scenarios the current shape models of asteroid 1998 ML14 (ref. 5) were selected. The shape models are polyhedra with triangular faces. The more detailed model, used as truth for thus study, has 16320 faces and 8612 vertices. The coarser representation has 1020 faces and 512 vertices. Both shapes are shown in Figure 3.

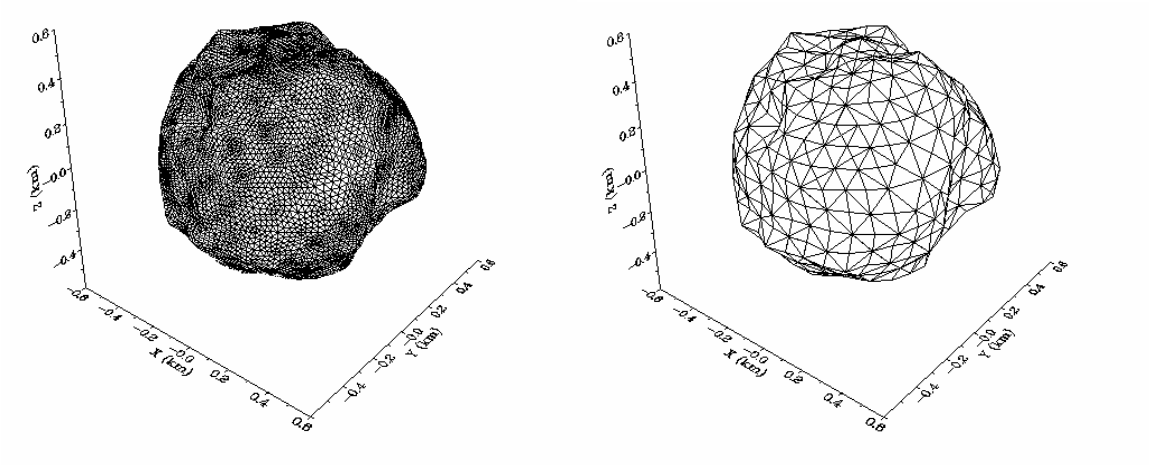

Figure 3. Reference (L) and Coarse (R) Shape Representations of Asteroid 1998 ML14

Numerical Evaluations

Across the three scenarios, it was determined that two types of evaluations were needed. Trajectory integrations of spacecraft and particles are the backbone of analyses and operations, so they were included to show the cumulative effect of gravity mismodeling upon these particular trajectories. Perturbations due to solar radiation pressure and third body effects were included. The mapping orbit was a 3km retrograde orbit in the terminator plane, with the spin axis at roughly 45 degrees to both the asteroid orbit plane and the terminator plane at epoch. The trajectory was integrated for two months, a duration intended to represent a long-duration mapping campaign.

In some implementations a variable-step integrator may be used, and the number of calls to the gravity model may be a function of the fidelity of the model itself. To isolate that effect in the overall performance evaluation, individual calls to the gravity model were made for a specific number of points. In the case of the mapping orbit, a set of 192 points, evenly spaced over a sphere at mapping orbit altitudes (with about a 10 degree spacing between adjacent points) was selected. In the hovering case, a grid with the same number of points was created, forming a box with dimensions about 5% of the body mean radius.

Both sets of evaluations were performed with the MONTE (Mission-analysis, Operations, and Navigation Toolkit Environment) software set developed at the Jet Propulsion Laboratory, using double precision code. In addition, cases were added that included (a) a best-fit homogeneous tri-axial ellipsoid, and (b) 4^{th} and 12^{th} order spherical harmonics that were computed from fits to the reference shape model.

RESULTS

Before the results can be evaluated, it is necessary to establish just how accurate the reference shape and the assumption of homogeneity can be in practice. In this evaluation, we assume that in a real mission we would have mass estimates based on initial flybys good to about 0.1%, which provides a threshold for mapping orbit accuracy. At the altitudes used in the hovering scenario, shape determination and rotation modeling errors will contribute to the error budget. With a reasonable camera and image collection campaign, shape uncertainties will be on the order of 20 cm horizontal, 5 cm vertical, and 3 mm point to point[4]. The corresponding spin pole errors will be no larger than 0.1 degrees (Ref. 6). On the surface, internal inhomogeneities and regolith distribution would be the leading causes of density variation, observed to be on the order of 1% at Eros (Ref. 7). The two conclusions to keep in mind are

(1) Modeling errors below 0.1% do not contribute much to the overall ability to predict spacecraft and particle trajectories in the planning phase,

(2) Navigation requirements in operations typically call for accelerations to be known to the 10^{-12} km/s2 level, or about .001% of the average acceleration encountered near the surface for the mass level considered in this study. Augmentations will have to be made to whatever gravity model strategy is selected (typically through the introduction of mascons or functional representations of density variation) for the hovering and surface scenarios.

Figure 4 shows the accuracy and relative runtime performance for the gravitational acceleration function calls for the various models at mapping orbit altitudes of 3 radii. The maximum and average errors and standard deviation of the errors are shown for each case. The two-term approximation (bottom right) gave nearly a 40% improvement in run time at essentially no cost in accuracy, for both the reference and coarse shape models. Going to the one-term approximation had only a fraction of that benefit, with an increased error level. The runtimes with the coarse shape model did seem to nearly scale as the number of vertices and shapes, while still performing at acceptable error levels for this particular shape choice. The absolute magnitude of the reference and coarse shape approximation cases does appear to be dominated by the L_e errors.

The ellipsoidal and spherical harmonic cases relative to each other seemed to perform as expected, with the higher error level partially attributed to challenges in properly applying the best-fit orientation parameters to the ellipsoid and harmonics in the integrator. Figure 5 shows the fit errors of the ellipse to the polyhedron vertices as a function of surface position, along with the region covered by the trajectory integrations (+/- 50 degrees).

It is difficult to concisely and clearly show the spatial distribution of gravity errors and their temporal effect on the integrated mapping orbit trajectory, since the cumulative position errors distort the ability to continue comparing instantaneous acceleration values. In Figure 6, the errors of the coarse shape model in latitude and longitude are shown as a function of time, and the large excursions are in phase with the equator crossings at East Longitudes between 0 and 90 degrees. One can see that the longitudinal errors reach peak values only over these equator crossings, while the latitude errors climb and fall with alternating ascending and descending crossings (keep in mind that the asteroid rotation period is much shorter than the spacecraft orbit period). Plots

[4] Robert Gaskell, personal communication.

like this are a useful tool for visualizing the mismodeling effects and provide a reasonable consistency check to the analyst.

Figure 4. Gravity Acceleration Errors vs. Runtimes

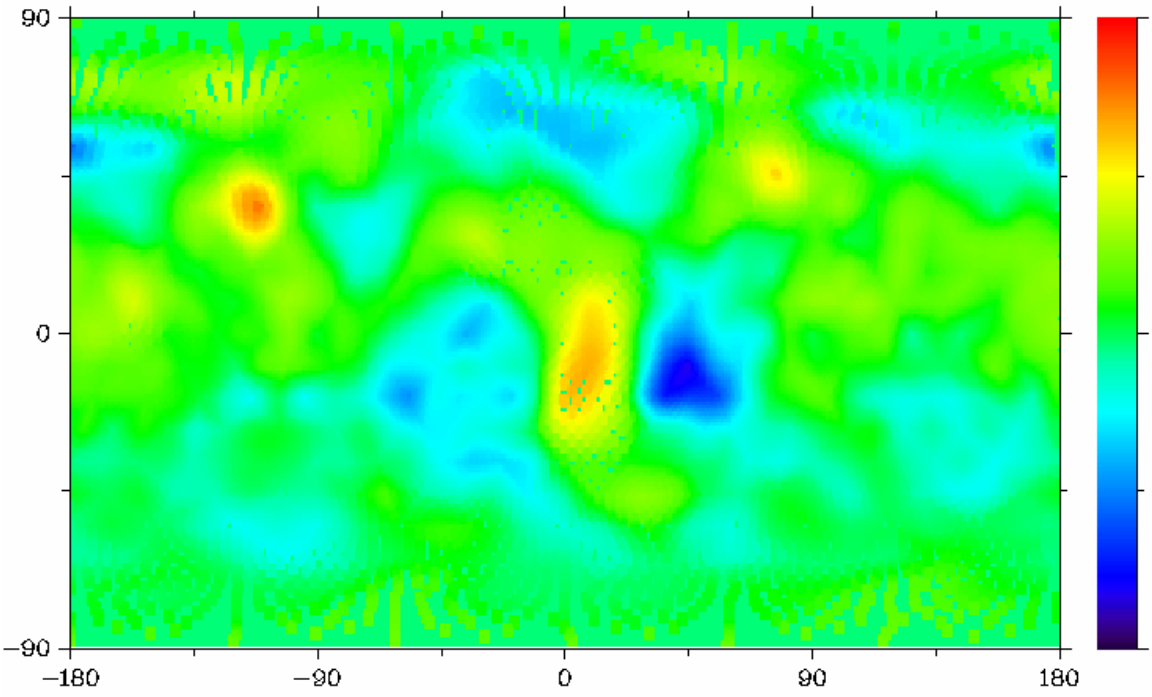

Figure 5. Normalized Ellipsoid Fit Errors

Figure 6. Trajectory Error Growth with the Ellipsoidal Model

Finally, the addition of the face and edge histories to the polyhedral library did improve run time with essentially no additional error. It is difficult to give a simple description of the average run time savings, since the histories will only help when the successive calls all have very similar position inputs. But in the most opportunistic cases, this technique alone can remove two thirds of the run time off of the original model (see Table 1). The benefits of these variations are largely independent of each other.

Case	Normalized Run Time (Reference = 1.0)
Coarse Shape Model	0.125
2-Term Taylor Series Approximation	0.615
Face / Edge Histories	0.364
Coarse Shape and Taylor Series	0.091
Coarse Shape and Histories	0.033
Taylor Series and Histories	0.0269
Coarse Shape, Taylor Series, and Histories	0.01

Table 1. Runtime Improvement Summary
(Relative to Reference Shape and Full Polyhedral Model)

CONCLUSIONS

The results show that the benefits to using Taylor series approximations and carrying the history of calculations from a previous call to a nearby point can range from 30 to 60 percent for each augmentation. The accuracy penalty for these augmentations is smaller than the uncertainties in the gravity field itself, so they warrant being included as part of gravity model software sets for small bodies. These augmentations are simple to describe and implement, altogether resulting in about 20 extra lines of code, and very few extra parameters for the software interface.

These improvements are but a small sample of the possibilities that warrant further investigation. These topics may lead to more complex, or more memory intensive augmentations, but not in all cases. Other methods and topics include, but are not limited to,

- Continued profiling of the polyhedral code, with emphasis on the remaining square root and triple product calls.
- The impact of all proposed augmentations on numerical stability, especially near the surface.
- Ellipsoidal harmonics, with emphasis on enhancing numerical robustness.

- Polyhedral gravity formulations that account for variations in density[5].

- Direct numerical integration of the mass distribution, packaged with a surface density model, as described in (Ref. 9).

- Robert Werner has also suggested reformulations of the polyhedral model so that ω_f remains essentially constant from the vantage point of the test mass.

ACKNOWLEDGEMENTS

This research was carried out at the Jet Propulsion Laboratory, California Institute of Technology, under a contract with the National Aeronautics and Space Administration. Reference herein to any specific commercial product, process, or service by trade name, trademark, manufacturer, or otherwise, does not constitute or imply its endorsement by the United States Government or the Jet Propulsion Laboratory, California Institute of Technology.

The author would like to gratefully acknowledge the help and contributions of the following people: Robert Werner and Steve Ostro at the Jet Propulsion Laboratory, and Dan Scheeres at the University of Michigan.

REFERENCES

1. S. Casotto and S. Musotto, "Methods for Copmuting the Potential of an Irregular, Mohogeneous, Solid Body and its Gradient," AIAA Paper 2000-4023.

2. L. A. Cangahuala and G. Minett, "An Orbit Design Method to Support Small Body Interior Radar Studies," 18th International Symposium on Space Flight Dynamics, Munich, Germany, 2004.

3. R. A. Werner and D. J. Scheeres, "Exterior Gravitation of a Polyhedron Derived and Compared with Harmonic and Mascon Gravitation Representations of Asteroid 4769 Castalia," *Celestial Mechanics and Dynamical Astronomy*, v. 65, pp. 313-344, 1997.

4. V. Pohánka, "Optimum Expression for Computation of the Gravity Field of a Homogeneous Polyhedral Body," *Geophysical Prospecting*, v. 26, pp. 733-751, 1988.

5. S. J. Ostro *et al*, "Radar Observations of Asteroid 1998 ML14," *Meteoritics and Planetary Science*, v. 36, no. 9, pp. 1225-1236, September 2001.

6. D. K. Yeomans, *et al*, "Radio Science Results During the NEAR-Shoemaker Spacecraft Rendezvous with Eros," Science, v. 289, pp. 2085-2088, 22 September 2000.

7. J. K. Miller et al, "Determination of Shape, Gravity, and Rotational State of Asteroid 433 Eros," *Icarus*, v. 155, pp. 3-17, 2002.

8. V. Pohánka, "Optimum Expression for Computation of the Gravity Field of a Polyhedral Body with Linearly Increasing Density," *Geophysical Prospecting*, v. 46, pp. 391-404, 1998.

[5] Pohánka, in (Ref. 8), revised his original polyhedral formulation to allow for a linear radial density function.

9. C. Weeks and J. K. Miller, “A Gravity Model for Navigation Close to Asteroids and Comets,” AAS/AIAA Space Flight Mechanics Meeting, San Antonio, Texas, 27-30 January 2002, AAS 02-140.